Bioelectrochemistry 133 (2020) 107458

Contents lists available at ScienceDirect

Bioelectrochemistry

journal homepage: www.elsevier.com/locate/bioelechem

Zinc oxide-gold nanocomposite as a proper platform for label-free DNA biosensor

Zahra Hatami, Elham Ragheb, Fahimeh Jalali *, Mahmoud Amouzadeh Tabrizi, Mojtaba Shamsipur

Department of Chemistry, Razi University, Kermanshah, Iran

ARTICLE INFO

Article history:
Received 11 October 2019
Received in revised form 6 January 2020
Accepted 6 January 2020
Available online 16 January 2020

Keywords:
Mycobacterium tuberculosis
ZnO nanoparticles
AuNPs
DNA biosensor
Label-free detection

ABSTRACT

In this study, a simple and cost-effective electrochemical DNA biosensor was developed for sensitive detection of mycobacterium tuberculosis (TB). Nanocomposite of zinc oxide (ZnO) and gold nanoparticles (AuNPs) was used as a platform for immobilizing thiolated TB DNA (probe DNA). ZnO was electrodeposited on a glassy carbon electrode by potentiostat electrolysis of Zn $(NO_3)_2$ solution at −1.0 V (vs. Ag/AgCl), then AuNPs were loaded as the second layer at −0.4 V from $HAuCl_4$ solution. Thiolated probe DNA was then covalently attached to AuNPs. Anodic peak current of $Fe(CN)_6^{3-/4-}$ was followed in hybridization experiments and a linear calibration curve was obtained in concentration range of 2.5–250 pM and limit of detection (LOD) of 1.8 pM for target DNA. The label-free TB biosensor exhibited high selectivity, suitable stability, and reproducibility.

1. Introduction

Mycobacterium tuberculosis (TB) causes tuberculosis, which most commonly affects the lungs. TB is transmitted via droplets from throat and lungs of infected individuals to healthy ones, and it is one of the deadliest diseases worldwide. According to The Centers for Disease Control and Prevention in 2014, 9.6 million individuals around the world contracted TB, 1.2 million of whom had HIV infection as well. People with HIV are 23 times more likely to develop TB compared to those without an HIV infection [1,2]. Therefore, developing sensitive, fast, and cost-effective methods of diagnosing Mycobacterium bacteria becomes crucial.

DNA detection methods for early diagnosis of diseases have attracted considerable attention [3,4]. DNA of TB has been detected by several techniques such as polymerase chain reaction [5,6], DNA microarray assay [7,8] and cycling probe technology [9]. However, the existing methods have various limitations such as complexity, long analysis time and high cost [10]. In contrast, electrochemical DNA biosensors are attractive alternatives, due to their simple application and low cost [11–14]. The performance of DNA electrochemical biosensors greatly depends on physical and chemical properties of the electrode surfaces [15–17]. Therefore a variety of materials have been used for construction of electrochemical biosensors to improve their characteristics [11,18–23]. Metal oxides have attracted considerable interest for electrode modification [24–27]. Among various metal oxides, zinc oxide (ZnO) has received much attention in biosensors because of desirable properties such as high surface area, nontoxicity, good biocompatibility, easy formation of stable nanostructures, and high electron communication ability. In the case of DNA biosensors, positively charged ZnO (isoelectric point 9.5 [28]) helps to hold negatively charged DNA on the electrode surface. It is also a good candidate for constructing future small integrated biosensor devices [29–35]. Different techniques have been used for synthesis of ZnO nanostructures including hydrothermal decomposition [36], thermal evaporation [37], chemical synthesis [38], precipitation [39] and crystallization [40] methods. Recently, electrochemical techniques have been used for growing ZnO nanostructures with different kinds of surface morphologies and shapes because these methods are very simple, fast and easy to control [41–43].

In the case of electro-inactive target compounds, a proper electrochemical indicator is required which produce a sensitive signal in response to the presence of target species. The electrochemical indicator has been used in two different ways; as one of the components of the modified electrode [44–47] in labelled biosensors, or as a part of the buffer solution in label-free biosensors. Due to the difficulties in attaching electrochemical indicators to electrodes, and possible effect on the biomolecule (DNA, enzyme, etc.) activity, it is preferred to apply label-free biosensors by using electrochemical indicators, such as $Fe(CN)_6^{3-/4-}$ [48,49], methylene blue [50], and $[Ru(NH_3)_6]^{3+}$ [51].

In this study, we report electrodeposition of ZnO-AuNPs on a glassy carbon electrode (GCE) for immobilization of single strand

* Corresponding author.
E-mail address: fahimeh41@gmail.com (F. Jalali).

https://doi.org/10.1016/j.bioelechem.2020.107458
1567-5394/

probe DNA of TB (ssDNA). To the best of our knowledge, this is the first application of metal oxides in voltammetric TB- biosensor. Hybridization of the target DNA (in sample solution), with ssDNA (on the electrode surface) occurred during the incubation time. As a result, the peak current of electrochemical indicator ($Fe(CN)_6^{3-/4-}$) decreased proportional to target DNA concentration. The proposed label-free DNA biosensor displayed high selectivity and sensitivity, wide linear range and picomolar LOD for TB- DNA.

2. Experimental section

2.1. Material and reagents

All reagents in the present study were of analytical grade and used without further purification. Double distilled water was used as solvent in all experiments. Potassium dihydrogen phosphate (KH_2PO_4), potassium nitrate (KNO_3), potassium chloride (KCl), zinc nitrate hexahydrate $Zn(NO_3)_2{\cdot}6H_2O$, potassium hexacyanoferrate (III) ($K_3[Fe(CN)_6]$) and potassium hexacyanoferrate (II) ($K_4[Fe(CN)_6]$) were purchased from Merck (Darmstadt, Germany). Gold (III) chloride trihydrate ($HAuCl_4{\cdot}3H_2O \geq 49.0\%$ Au basis) was obtained from Sigma-Aldrich (USA). DNA oligonucleotides were purchased from Fazabiotech Co. (Tehran, Iran). Their sequences were as follows:

Probe DNA (ssDNA): 5′- GGTGAGGTCTGCTACCCAC-3′- SH [52]
Target DNA: 5′-GTGGGTAGCAGACCTCACC-3′
Double-base mismatched DNA: 5′- GAGGCTAGCAGACCTCACC-3′
Three-base mismatched DNA: 5′- GAGGCTAGAAGACCTCACC-3′
Non-complementary DNA: 5′- AATCTCATGGCCGATTCGT-3′.

2.2. Apparatus and measurements

Cyclic voltammetry (CV), electrochemical impedance spectroscopy (EIS) and differential pulse voltammetry (DPV) were carried out using a μ-Autolab electrochemical system (Eco Chemie B. V., Utrecht, Netherlands). For data acquisition and processing, NOVA 1.8 software was used. The working electrode was a glassy carbon electrode, GCE (i.d. = 3.0 mm) modified with AuNPs, ZnO, and ssDNA (ssDNA/ZnO-AuNPs /GCE), a Pt wire was applied as auxiliary, and Ag/AgCl (KCl, 3 M) as reference electrode.

The bias potential for EIS experiments was 0.28 V, the amplitude of the alternate voltage was 10 mV and frequency range of 100 kHz to 0.1 Hz was applied. Scanning electron microscopy (SEM) images were obtained by a Tescan instrument, Model MIRA3 (Czech Republic). Atomic force microscopy (AFM) images were obtained using a DME Dual Scope Scanner DS 95–200 (Herlev, Denmark). Energy – dispersive X-ray spectroscopy (EDX Oxford Instruments, UK) was used in secondary electron mode (SE) to obtain elemental maps of the composites.

2.3. Preparation of ssDNA/ZnO-AuNPs /GCE and hybridization with target DNA

To obtain a mirror finish, the surface of GCE was polished by alumina (0.3, 0.1 and 0.05 μm mesh sizes) slurry and subsequently cleaned under ultrasonication in water–ethanol solution (1:1). Deposition of ZnO was carried out in a mixture of $Zn(NO_3)_2{\cdot}6H_2O$ (0.5 mM) and KNO_3 (0.1 M) by potentiostat electrolysis at −1.0 V (vs. Ag/AgCl, KCl 3 M) during 300 s [53]. Then the electrode was washed with a plenty of double distilled water and dried in an oven (85 °C for 15 min) to obtain ZnO/GCE. To deposit AuNPs, ZnO/GCE was immersed in $HAuCl_4$ solution (0.5 mM) containing 0.1 M KCl, and a constant potential at − 0.4 V (vs. Ag/AgCl, KCl 3 M) was applied for 600 s [54]. Next, the prepared electrode (AuNPs/ZnO/GCE) was washed with phosphate buffer solution (PBS) and immersed in probe DNA solution (1 μM in PBS 0.05 M, pH 7.0) for 12 h to obtain ssDNA/AuNPs/ZnO/GCE. Finally, the electrode was thoroughly washed with double distilled water, and stored in PBS (0.1 M, pH 7.0) at 4 °C when not in use.

TB-DNA (target DNA) in sample solutions was determined by DPV on ssDNA/AuNPs/ZnO/GCE, in $[Fe(CN)_6]^{3-/4-}$ (5.0 mM). The difference between peak currents in the two steps (absence and presence of target DNA, ΔIp) was used as analytical signal. Schematic representation of the electrode preparation steps (Scheme 1) shows the procedure, clearly.

3. Results and discussion

3.1. Characterization of the modified electrodes

Electrodeposition of ZnO nanostructures from nitrate baths has been reported to occur via the following reactions [53]:

$$Zn(NO_3)_2 \rightarrow Zn^{2+} + 2NO_3^- \quad (1)$$

$$NO_3^- + H_2O + 2e \rightarrow NO_2^- + 2OH^- \quad (2)$$

$$Zn^{2+} + 2OH^- \leftrightarrow Zn(OH)_2 \quad (3)$$

Zinc hydroxide formed through Eq. (3) is transformed into ZnO at elevated temperatures (in this study, 85 °C):

$$Zn(OH)_2 \rightarrow ZnO + H_2O \quad (4)$$

The surface of ZnO/GCE was observed by SEM (Fig. 1A) which showed the uniform distribution of ZnO nanoparticles. This modified electrode served as a proper substrate for deposition of AuNPs (Fig. 1B) but the presence of AuNPs is not distinguishable in SEM images due to their small size. AFM image of AuNPs/ZnO/GCE (Fig. S1, Supp.docx) was also recorded which showed 3D structure of the modified electrode. The nano-size ZnO, could dramatically enhance the active surface area of GCE and provide a suitable environment for AuNPs' deposition. Further morphological study of ZnO/GCE by BET analysis (Fig. S1, Supp. docx) showed both micropores and mesopores (BJH-plot) with a wide distribution which is consistent with the N_2 adsorption/desorption isotherm [55]. The BET surface area, BJH adsorption average pore width and pore volume of ZnO/GCE were 7.35 $m^2\ g^{-1}$, 1.82 nm and 0.081 $cm^3 g^{-1}$, respectively. Finally, EDX elemental mapping clearly showed the presence of Zn, and Au in the prepared nanocomposite (Fig. 1C).

The interface properties of modified electrodes were studied by CV and EIS (Fig. 2). As is shown in Fig. 2A, largely decreased peak currents and increased peak to peak separation for $Fe(CN)_6^{3-/4-}$ was recorded on ZnO/GCE (curve b) compared to GCE (curve a). This observation may be related to the semiconducting nature of ZnO with decreased conductivity. After electrochemical deposition of AuNPs, the redox peaks of $Fe(CN)_6^{3-}/^{4-}$ were restored (curve c), which indicates enhanced electron transfer rate brought about by AuNPs. Nyquist plots were recorded for different modified electrodes (Fig. 2B). In comparison with GCE (curve a), the radius of semicircle (proportional to electron transfer resistance, R_{ct}) for ZnO/GCE (curve b) increased from 171 Ω to 10930 Ω (decreased rate of electron transfer), which shows reduced conductivity. However, after electrochemical deposition of AuNPs (curve c), R_{ct} decreased to 145 Ω, which demonstrated effective facilitation of electron transfer due to the presence of conducting bridges of AuNPs.

The effective surface area of GCE, AuNPs /GCE and AuNPs/ZnO / GCE were calculated in $K_3[Fe(CN)_6]$ solution by applying CV at different scan rates. According to Randles–Sevcik equation:

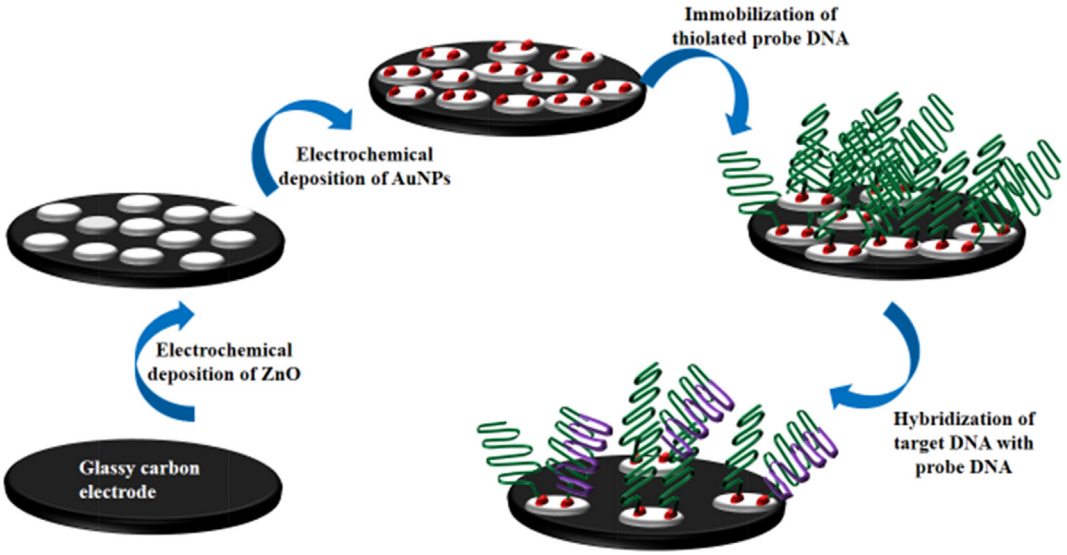

Scheme 1. Representation of electrode modification steps.

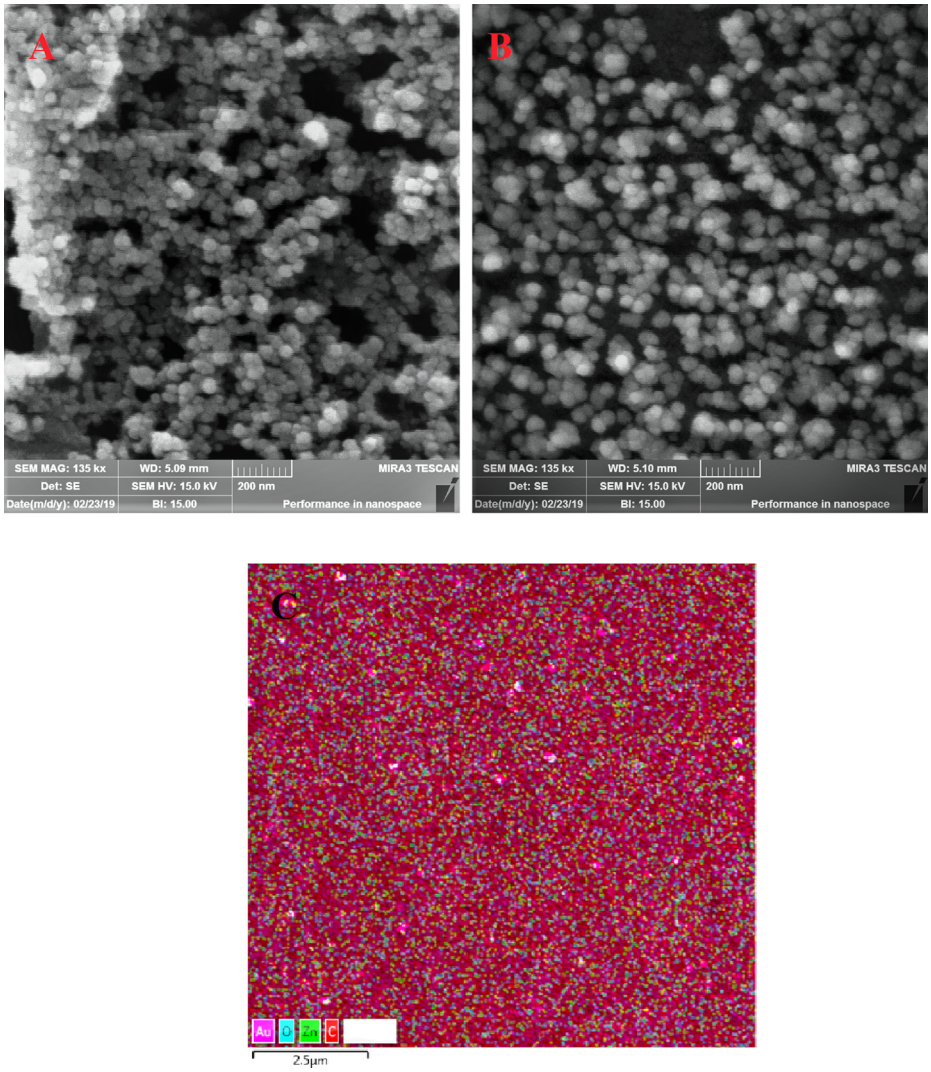

Fig. 1. SEM images of (A) ZnO/GCE and (B) AuNPs/ZnO/GCE; (C) EDX map recorded at AuNPs/ZnO/GCE.

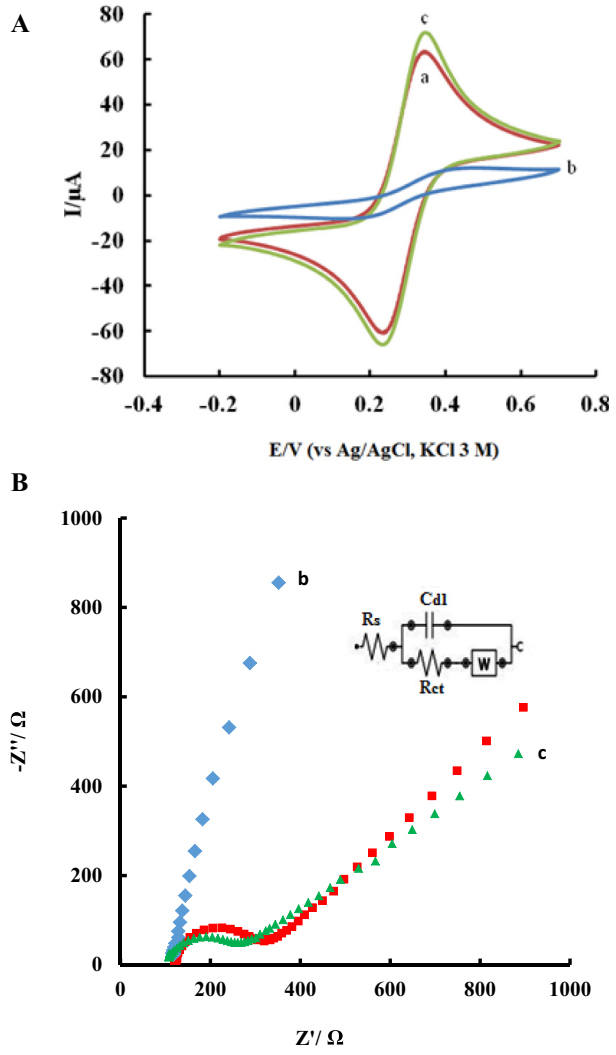

Fig. 2. (A) Cyclic voltammograms, and (B) Nyquist plots of (a) GCE, (b) ZnO/GCE and (c) AuNPs/ZnO/GCE recorded in Fe $(CN)_6^{3-}/^{4-}$ solution (5.0 mM in 0.1 M KCl); inset is the equivalent circuit. R_s = solution resistance, R_{ct} = electron transfer resistance, C_{dl} = double layer capacitance, W = Warburg impedance.

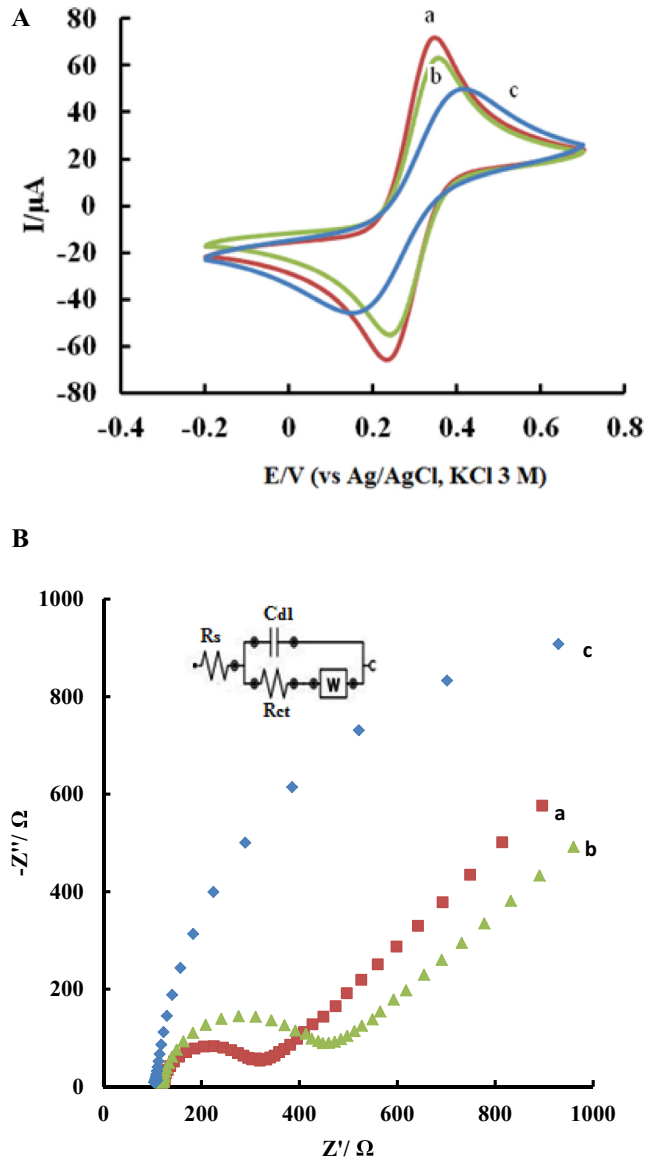

Fig. 3. (A) Cyclic voltammograms, and (B) Nyquist plots of (a) AuNPs/ZnO/GCE, (b) ssDNA/AuNPs/ZnO/GCE, (c) dsDNA/AuNPs/ZnO/GCE recorded in Fe $(CN)_6^{3-}/^{4-}$ solution (5.0 mM in 0.1 M KCl); inset is the equivalent circuit. R_s = solution resistance, R_{ct} = electron transfer resistance, C_{dl} = double layer capacitance, W = Warburg impedance.

$$I_p = \left(2.69 \times 10^5\right) n^{3/2} A D^{1/2} C \upsilon^{1/2} \quad (5)$$

I_p is proportional to the square root of scan rate, υ for a diffusion-controlled current. In this equation, I_p is the peak current, n is the number of electrons transferred, A is the electrode surface area, D is diffusion coefficient, and C is $Fe(CN)_6^{3-}/^{4-}$ concentration. From the slope of linear plot of I_p vs. $\upsilon^{1/2}$, effective surface area was calculated as 0.031 cm^2 for GCE, 0.054 cm^2 for AuNPs/GCE and 0.083 cm^2 for AuNPs/ZnO/GCE, which indicates more AuNPs were deposited on ZnO/GCE than GCE due to the large surface area presented by ZnO nanostructures. The cyclic voltammograms and Randles-Sevcik plots are reported (Fig. S2, Supp.docx).

Similar CV experiments were carried out on ssDNA/AuNPs/ZnO/GCE before and after hybridization with target DNA (Fig. 3). As can be seen, when ssDNA was accumulated on AuNPs/ZnO/GCE, the peak current decreased (curve b). Moreover, after hybridization with target DNA, the peak current decreased, significantly (curve c). It may be due to increased number of negative phosphate groups after hybridization, which resulted in strong repulsion of Fe $(CN)_6^{3-}/^{4-}$ from electrode. As a result, the peak current decreased while peak to peak separation increased (curve c). Another reason for this observation could be the less accessible active sites for Fe $(CN)_6^{3-}/^{4-}$ on electrode surface after DNA hybridization [56,57].

The corresponding EIS spectra were recorded (Fig. 3B), which showed increased R_{ct} from 145 to 292 Ω when probe DNA was immobilized on AuNPs/ZnO/GCE (curve b compared to a). Hybridization with target DNA resulted in largely increased R_{ct} to 1903 Ω (curve c), which is consistent with CV results.

These observations demonstrated that hybridization of DNA at ssDNA/AuNPs/ZnO/GCE is accompanied by a large decrease in peak current of $Fe(CN)_6^{3-}/^{4-}$(increased ΔIp), which can be utilized in label-free voltammetric detection of target DNA.

To investigate the role of deposited ZnO on biosensor performance, ZnO-modified (ssDNA/AuNPs/ZnO/GCE) and ZnO-free (ssDNA/AuNPs/GCE) electrodes were compared. The former showed much larger peak current for $Fe(CN)_6^{3-}/^{4-}$ in comparison with ZnO-free electrode (curves a and b in Fig. 4A). The improvement may be due to the porous structure of ZnO which increased

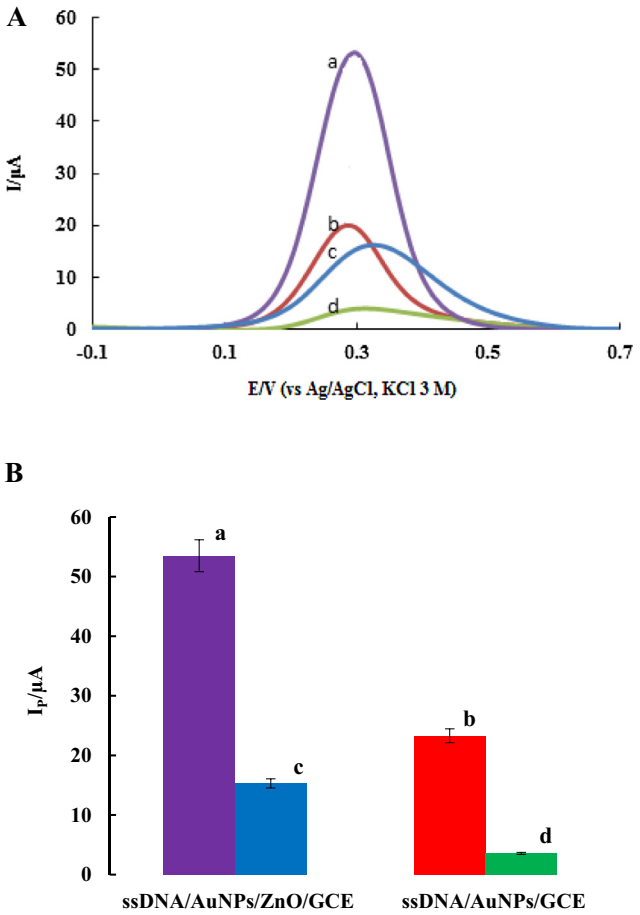

Fig. 4. (A) Comparison between DPVs of modified electrodes ssDNA/AuNPs/ZnO/GCE and ssDNA/AuNPs/GCE in the absence (a, b) and presence (c, d) of complementary DNA. (B) Comparison of peak currents based on DPVs in (A).

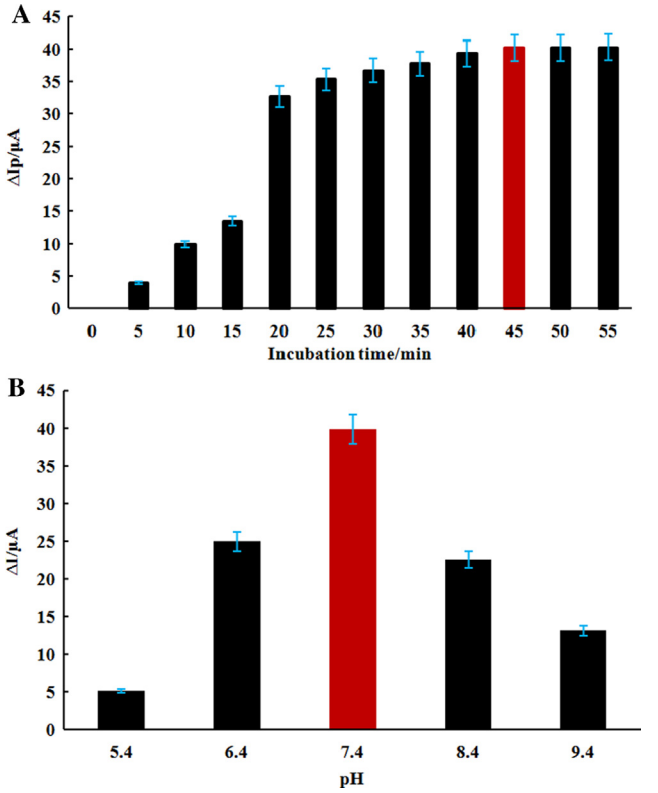

Fig. 5. Effect of (A) incubation time, and (B) pH, on the response of ssDNA/AuNPs/ZnO/GCE to target DNA (100 pM) recorded in Fe $(CN)_6^{3-}/^{4-}$ solution (5.0 mM in 0.1 M KCl).

amount of deposited AuNPs, and also good electrical mobility brought about by ZnO nanoparticles [29]. On the other hand, ZnO with a partially positive charge at pH 7.4 (isoelectric point 9.5), absorbs negatively charged DNA, i.e., more probe DNA accumulated at ZnO-modified electrode. The result is hybridization with more target DNA, and larger ΔIp on ssDNA/AuNPs/ZnO/GCE compared to ssDNA/AuNPs/GCE.

3.2. Determination of target DNA

As discussed above, the peak current of Fe (CN)6 $^{3-/4-}$ decreased in the presence of target DNA due to hybridization, so the peak current change (ΔIp) was used as the analytical signal for determination of target DNA. To use ssDNA/AuNPs/ZnO/GCE as a DNA biosensor for tracking TB, the effect of incubation time, and pH on ΔIp were investigated. During incubation time, hybridization proceeded to a significant degree up to 45 min but remained nearly unchanged at longer times (Fig. 5A), so the biosensor was incubated with sample solution for 45 min before electrochemical analysis. Fig. 5B shows the response of DNA biosensor to different pH values. By increasing pH from 5.4 to 7.4, ΔIp increased and then decreased at alkaline solutions, due to optimized configuration and function of biological compounds at physiological pH 7.4.

In the next step, a calibration curve was obtained in optimized conditions from DPV curves by using different concentrations of target DNA. As can be seen from Fig. 6 (A and B), DPV peak current decreased linearly with increasing target DNA concentration (logarithmic scale) over the range of 2.5–250 pM with two linear segments: ΔI_p (μA) = 30 log [DNA](pM) −1, and ΔI_p (μA) = 10 log [DNA](pM) −20. The limit of detection (LOD) of 1.18 pM was calculated (3S/N).

The smaller slope of the calibration curve in higher concentrations of target DNA is due to the limited number of available probe DNA on electrode surface for hybridization. Therefore, smaller changes in peak currents of Fe $(CN)_6^{3-}/^{4-}$ were observed, and the slope of the second linear segment of calibration curve decreased.

The high sensitivity obtained in DNA analysis is due to the synergistic effect of ZnO and AuNPs that led to increased surface area of the modified electrode, and resulted in higher loadings of thiolated probe DNA on AuNPs/ZnO/GCE compared to GCE. In addition, better electrical communication brought about by ZnO and AuNPs increased the method sensitivity.

To investigate the method selectivity, double-base mismatched (DMM), three-base mismatched (TMM) or non-complementary (NCMM) strands (each 100 pM) were examined as sample solutions (Fig. 7). The corresponding ΔIp values were 48.8% (DMM), 27.0% (TMM) and 4.93% (NCMM) compared to an equimolar concentration of completely matched DNA (target), which shows the recognition ability of the peoposed biosensor towards the DNA of TB.

Three freshly prepared modified electrodes were applied to evaluate the method reproducibility. Relative standard deviation (RSD %) for DPV determination of target DNA (100 pM) was 2.97%, which shows excellent reproducibility of the biosensor.

Long-term stability of DNA biosensor was investigated by storing the electrode at 4 °C (in PBS 0.1 M, pH7.0) for 10 days. The measured ΔI_p decreased only 4.25% after 10 days, demonstrating high stability of the electrode.

Analytical performance of the proposed TB-DNA biosensor was compared with other similar TB biosensors in literature. As shown

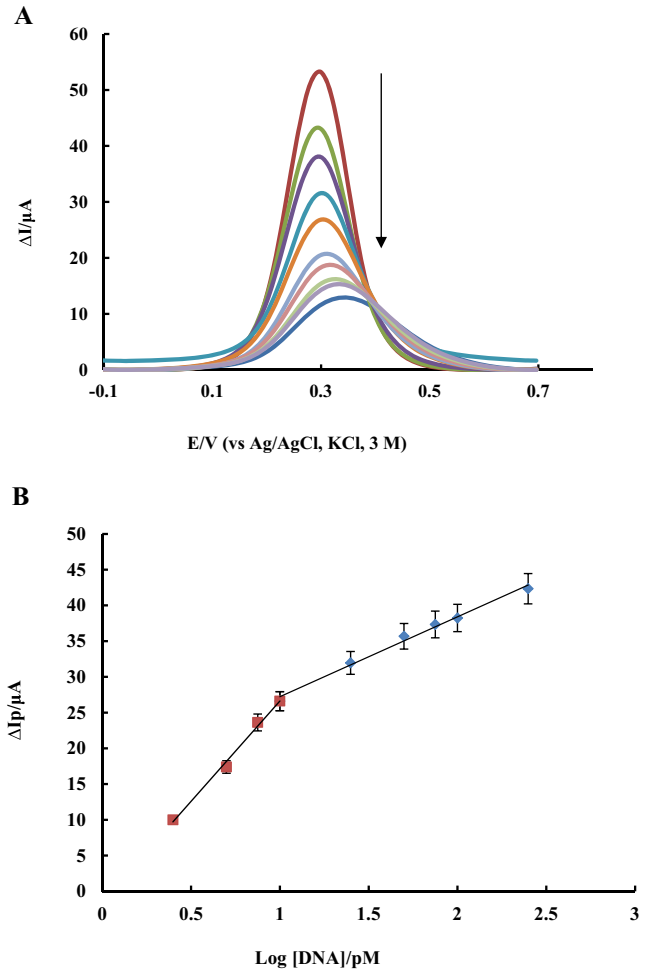

Fig. 6. (A) DPV results for ssDNA/AuNPs/ZnO/GCE incubated with various concentrations of target DNA; (B) calibration curve (ΔI_p versus log [DNA]).

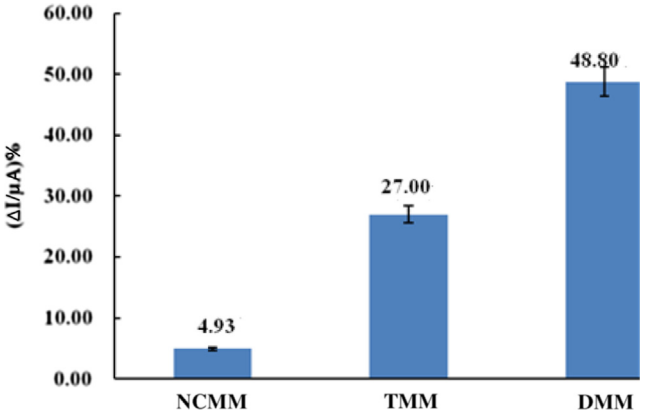

Fig. 7. Comparison of hybridization signal intensities for ssDNA/AuNPs/ZnO/GCE in the presence of double-base mismatched (DMM), three-base mismatched (TMM) and non-complementary sequences (NCMM) oligonucleotides. The concentration of each compound was 100 pM.

in Table 1, detection limit and linear range for the proposed DNA biosensor were comparable or better than previous reports. In comparison with MWCNTs-PPy-PAMAM-Fc-ssDNA [58] and GCE/rGO–AuNPs-DNA-Au–PANI [13], the proposed DNA biosensor has some advantages, such as reproducibility, facile operation and cost-effectiveness.

Table 1
Comparison of the analytical performance of the different DNA biosensors.

Modified electrode	Method	Liner range	Limit of detection	References
GCE/rGO–AuNPs-DNA-Au–PANI	DPV	1.0 fM-1.0 nM	–	[13]
AuNTsA/ss DNA	DPV	0.01–100 nM	0.05 nM	[12]
MWCNTs-PPy-PAMAM-Fc-ssDNA	SWV	0.001 fM-100 nM	0.3 fM	[58]
Reduced graphene oxide/quantum dots	DPV	10 pM–100 nM	0.895 pM	[59]
acpcPNA	EIS	2–200 nM	1.24 nM	[60]
GCE-ZnO-AuNPs-ssDNA	DPV	2.5–250 pM	1.8 pM	This work

rGO: reduced graphene oxide; PANI: polyaniline; AuNTsA: gold nanotubes array; MWCNTs: multiwalled carbon nanotubes; PPy: polypyrrole; PAMAM: poly(amidoamine) dendrimers; Fc: ferrocene; acpcPNA: pyrrolidinyl peptide nucleic acid

Table 2
Measurements of TB-DNA in a mixture of target, DMM, TMM, and NCMM sequences by using the proposed method.

Sample no.	Added amount of target DNA (M)	Found amount of target DNA (M)[a]	Recovery (%)
1	2.50×10^{-12}	$(2.51 \pm 0.12) \times 10^{-12}$	100.4
2	2.50×10^{-11}	$(2.42 \pm 0.09) \times 10^{-11}$	96.8

[a] Average of 3 replicate measurements for each sample.

3.3. Analytical application of the DNA biosensor

A great feature of the designed DNA biosensor was its selectivity towards the target DNA in a mixture with DMM, TMM, and NCMM. A mixture containing oligonucleotides DMM, TMM, and NCMM (each 100 pM) was prepared. The target DNA (100 pM) was added and measured using the proposed method. As can be seen in Table 2, high accuracy is observed in measuring TB-DNA. These results showed that the proposed biosensor could be useful in real clinical samples for detection of TB- DNA.

4. Conclusions

A simple, cost effective and sensitive label-free electrochemical DNA biosensor (ssDNA/AuNPs/ZnO/GCE) was constructed for Mycobacterium tuberculosis bacteria (TB). The study revealed the usefulness of ZnO nanoparticles for electrode modification in biosensor application. The synergistic effect between ZnO and AuNPs in the nanocomposite led to distinct augmentation in response (ΔIp) to target DNA. A ~~sensitive~~ calibration curve was obtained for TB-DNA in the concentration range of 2.5–250 pM with a limit of detection of 1.8 pM. After 10 days, the response drift of the biosensor was about 4%, which indicates its long-term stability. The construction procedure showed excellent reproducibility (2.97% for 3 electrodes). Good selectivity towards target DNA was observed in the mixture with non-complementary DNA strands.

Declaration of Competing Interest

The authors declare that they have no known competing financial interests or personal relationships that could have appeared to influence the work reported in this paper.

Acknowledgements

The authors acknowledge the research council of Razi University for its financial support. The authors are also thankful from Miss Zhina Jalali for her professional work on language editing.

Appendix A. Supplementary material

Supplementary data to this article can be found online at https://doi.org/10.1016/j.bioelechem.2020.107458.

References

[1] E. Torres-Chavolla, E.C. Alocilja, Nanoparticle based DNA biosensor for tuberculosis detection using thermophilic helicase-dependent isothermal amplification, Biosens. Bioelectron. 26 (2011) 4614–4618.
[2] R. Mishra, P. Shukla, W. Huang, N. Hu, Gene mutations in Mycobacterium tuberculosis: multidrug-resistant TB as an emerging global public health crisis, Tuberculosis 95 (2015) 1–5.
[3] B. Rafique, M. Iqbal, T. Mehmood, M.A. Shaheen, Electrochemical DNA biosensors: a review, Sensor Rev. 39 (2019) 34–50.
[4] P. He, Y. Xu, Y. Fang, A review: electrochemical DNA biosensors for sequence recognition, Anal. Lett. 38 (2005) 2597–2623.
[5] R. Sanjuan-Jimenez, P. Morata, P. Bermúdez, M.J. Bravo, J.D. Colmenero, Comparative clinical study of different multiplex real time PCR strategies for the simultaneous differential diagnosis between extrapulmonary tuberculosis and focal complications of brucellosis, PLoS Negl. Trop. Dis. 7 (2013) e2593.
[6] V. Vinuesa, R. Borrás, M.L. Briones, M.Á. Clari, V. Cresencio, E. Giménez, C. Muñoz, R. Oltra, E. Servera, T. Scheelje, Performance of a highly-sensitive mycobacterium tuberculosis complex real-time PCR assay for the diagnosis of pulmonary tuberculosis in a low prevalence setting: a prospective intervention study, J. Clin. Microbiol. JCM (2018) 00116–00118.
[7] M. Fukushima, K. Kakinuma, H. Hayashi, H. Nagai, K. Ito, R. Kawaguchi, Detection and identification of mycobacterium species isolates by DNA microarray, J. Clin. Microbiol. 41 (2003) 2605–2615.
[8] A. Gaber, H. Hamed, E. Elsawy, Comparison between real-time polymerase chain reaction and DNA-microarray in detection and identification of mycobacterium species, Gen. Mol. Res. 16 (2017) 1–8.
[9] R. Pahwa, S. Hedau, S. Jain, N. Jain, V.M. Arora, N. Kumar, B.C. Das, Assessment of possible tuberculous lymphadenopathy by PCR compared to non-molecular methods, J. Med. Microbiol. 54 (2005) 873–878.
[10] F.A. Drobniewski, M. Caws, A. Gibson, D. Young, Modern laboratory diagnosis of tuberculosis, Lancet Infect. Dis. 3 (2003) 141–147.
[11] C. Thiruppathiraja, S. Kamatchiammal, P. Adaikkappan, D.J. Santhosh, M. Alagar, Specific detection of mycobacterium sp. genomic DNA using dual labeled gold nanoparticle based electrochemical biosensor, Anal. Biochem. 417 (2011) 73–79.
[12] S.R. Torati, V. Reddy, S.S. Yoon, C. Kim, Electrochemical biosensor for Mycobacterium tuberculosis DNA detection based on gold nanotubes array electrode platform, Biosens. Bioelectron. 78 (2016) 483–488.
[13] C. Liu, D. Jiang, G. Xiang, L. Liu, F. Liu, X. Pu, An electrochemical DNA biosensor for the detection of Mycobacterium tuberculosis, based on signal amplification of graphene and a gold nanoparticle-polyaniline nanocomposite, Analyst 139 (2014) 5460–5465.
[14] M. Amouzadeh Tabrizi, M. Shamsipur, A label-free electrochemical DNA biosensor based on covalent immobilization of salmonella DNA sequences on the nanoporous glassy carbon electrode, Biosens. Bioelectron. 69 (2015) 100–105.
[15] M. Wang, C. Sun, L. Wang, X. Ji, Y. Bai, T. Li, J. Li, Electrochemical detection of DNA immobilized on gold colloid particles modified self-assembled monolayer electrode with silver nanoparticle label, J. Pharm. Biomed. Anal. 33 (2003) 1117–1125.
[16] Y. Li, X. Teng, K. Zhang, R. Deng, J. Li, RNA strand displacement responsive CRISPR/Cas9 system for mRNA sensing, Anal. Chem. 91 (2019) 3989–3996.
[17] H. Yang, W. Zhao, S. Deng, K. Zhang, Z. Zhao, R. Deng, Q. He, J. Li, Intrinsic conformation-induced fluorescence resonance Energy Transfer Aptasensor, ACS Appl. Bio Mater. (2019).
[18] H. Peng, L. Zhang, C. Soeller, J. Travas-Sejdic, Conducting polymers for electrochemical DNA sensing, Biomaterials 30 (2009) 2132–2148.
[19] V. Rai, J. Deng, C.-S. Toh, Electrochemical nanoporous alumina membrane-based label-free DNA biosensor for the detection of Legionella sp, Talanta 98 (2012) 112–117.
[20] J. Yang, T. Yang, Y. Feng, K. Jiao, A DNA electrochemical sensor based on nanogold-modified poly-2,6-pyridinedicarboxylic acid film and detection of PAT gene fragment, Anal. Biochem. 365 (2007) 24–30.
[21] W. Zhang, P. Zong, X. Zheng, L. Wang, An enhanced sensing platform for ultrasensitive impedimetric detection of target genes based on ordered FePt nanoparticles decorated carbonnanotubes, Biosens. Bioelectron. 42 (2013) 481–485.
[22] Z. Zhang, L. Luo, G. Chen, Y. Ding, D. Deng, C. Fan, Tryptamine functionalized reduced graphene oxide for label-free DNA impedimetric biosensing, Biosens. Bioelectron. 60 (2014) 161–166.
[23] L. Zhu, L. Luo, Z. Wang, DNA electrochemical biosensor based on thionine-graphene nanocomposite, Biosens. Bioelectron. 35 (2012) 507–511.
[24] P.R. Solanki, A. Kaushik, V.V. Agrawal, B.D. Malhotra, Nanostructured metal oxide-based biosensors, NPG Asia Mater 3 (2011) 17–24.
[25] M. Das, G. Sumana, R. Nagarajan, B.D. Malhotra, Application of nanostructured ZnO films for electrochemical DNA biosensor, Thin Solid Films 519 (2010) 1196–1201.
[26] M. Tak, V. Gupta, M. Tomar, Flower-like ZnO nanostructure based electrochemical DNA biosensor for bacterial meningitis detection, Biosens. Bioelectron. 59 (2014) 200–207.
[27] P.M. Levine, P. Gong, R. Levicky, K.L. Shepard, Real-time, multiplexed electrochemical DNA detection using an active complementary metal-oxide-semiconductor biosensor array with integrated sensor electronics, Biosens. Bioelectron. 24 (2009) 1995–2001.
[28] S.A. Kumar, S.M. Chen, Nanostructured zinc oxide particles in chemically modified electrodes for biosensor applications, Anal. Lett. 41 (2008) 141–158.
[29] S.K. Arya, S. Saha, J.E. Ramirez-Vick, V. Gupta, S. Bhansali, S.P. Singh, Recent advances in ZnO nanostructures and thin films for biosensor applications: review, Anal. Chim. Acta 737 (2012) 1–21.
[30] A. Fulati, S.M. Ali, M.H. Asif, M. Willander, C. Brännmark, P. Strålfors, S.I. Börjesson, F. Elinder, B. Danielsson, An intracellular glucose biosensor based on nanoflake ZnO, Sens. Actuat. B: Chem. 150 (2) (2010) 673–680.
[31] V. Gupta, ZnO based third generation biosensor, Thin Solid Films 519 (2010) 1141–1144.
[32] G.-Q. Mo, J.-S. Ye, W.-D. Zhang, Unusual electrochemical response of ZnO nanowires-decorated multiwalled carbon nanotubes, Electrochim. Acta 55 (2009) 511–515.
[33] W. Zhang, T. Yang, D.M. Huang, K. Jiao, Electrochemical sensing of DNA immobilization and hybridization based on carbon nanotubes/nano zinc oxide/chitosan composite film, Chin. Chem. Lett. 19 (2008) 589–591.
[34] Z. Han, M. Luo, L. Chen, H. Pan, J. Chen, C. Li, A photoelectrochemical biosensor for determination of DNA based on flower rod-like zinc oxide heterostructures, Microchim. Acta 184 (2017) 2541–2549.
[35] A.M. Mohammed, I.J. Ibraheem, A.S. Obaid, M. Bououdina, Nanostructured ZnO-based biosensor: DNA immobilization and hybridization, Sens. Bio-Sens. Res. 15 (2017) 46–52.
[36] B. Fang, C. Zhang, G. Wang, M. Wang, Y. Ji, A glucose oxidase immobilization platform for glucose biosensor using ZnO hollow nanospheres, Sens. Actuat. B: Chem. 155 (2011) 304–310.
[37] A. Wei, X.W. Sun, J.X. Wang, Y. Lei, X.P. Cai, C.M. Li, Z.L. Dong, W. Huang, Enzymatic glucose biosensor based on ZnO nanorod array grown by hydrothermal decomposition, Appl. Phys. Lett. 89 (2006) 123902.
[38] X. Ren, D. Chen, X. Meng, F. Tang, X. Hou, D. Han, L. Zhang, Zinc oxide nanoparticles/glucose oxidase photoelectrochemical system for the fabrication of biosensor, J. Coll. Interf. Sci. 334 (2009) 183–187.
[39] J. Wang, Z. Gao, Z. Li, B. Wang, Y. Yan, Q. Liu, T. Mann, M. Zhang, Z. Jiang, Green synthesis of graphene nanosheets/ZnO composites and electrochemical properties, J. Solid State Chem. 184 (2011) 1421–1427.
[40] L. Zhang, Z. Chen, Y. Tang, Z. Jia, Low temperature cathodic electrodeposition of nanocrystalline zinc oxide thin films, Thin Solid Films 492 (2005) 24–29.
[41] M. Skompska, K. Zarębska, Electrodeposition of ZnO nanorod arrays on transparent conducting substrates–a review, Electrochim. Acta 127 (2014) 467–488.
[42] A. Stafiniak, B. Boratyński, A. Baranowska-Korczyc, A. Szyszka, M. Ramiączek-Krasowska, J. Prażmowska, K. Fronc, D. Elbaum, R. Paszkiewicz, M. Tłaczała, A novel electrospun ZnO nanofibers biosensor fabrication, Sens. Actuat. B: Chem. 160 (2011) 1413–1418.
[43] Y. Leprince-Wang, S. Bouchaib, T. Brouri, M. Capo-Chichi, K. Laurent, J. Leopoldes, S. Tusseau-Nenez, L. Lei, Y. Chen, Fabrication of ZnO micro- and nano-structures by electrodeposition using nanoporous and lithography defined templates, Mater. Sci. Eng. B 170 (2010) 107–112.
[44] Y. Liu, N. Tuleouva, E. Ramanculov, A. Revzin, Aptamer-based electrochemical biosensor for interferon gamma detection, Anal. Chem. 82 (2010) 8131–8136.
[45] S. Centi, L. Bonel Sanmartin, S. Tombelli, I. Palchetti, M. Mascini, Detection of C reactive protein (CRP) in serum by an electrochemical aptamer-based sandwich assay, Electroanalysis 21 (2009) 1309–1315.
[46] H. Karimi-Maleh, O.A. Arotiba, Simultaneous determination of cholesterol, ascorbic acid and uric acid as three essential biological compounds at a carbon paste electrode modified with copper oxide decorated reduced graphene oxide nanocomposite and ionic liquid, J. Coll. Interf. Sci. 560 (2020) 208–212.
[47] H. Karimi-Maleh, C.T. Fakude, N. Mabuba, G.M. Peleyeju, O.A. Arotiba, The determination of 2-phenylphenol in the presence of 4-chlorophenol using nano-Fe_3O_4/ionic liquid paste electrode as an electrochemical sensor, J. Coll. Interf. Sci. 554 (2019) 603–610.
[48] L. Li, H. Zhao, Z. Chen, X. Mu, L. Guo, Aptamer biosensor for label-free square-wave voltammetry detection of angiogenin, Biosens. Bioelectron. 30 (2011) 261–266.
[49] N. Oliveira, E. Costa-Rama, S. Viswanathan, C. Delerue-Matos, L. Pereira, S. Morais, Label-free voltammetric immunosensor for prostate specific antigen detection, Electroanalysis 30 (2018) 2604–2611.
[50] F. Yan, F. Wang, Z. Chen, Aptamer-based electrochemical biosensor for label-free voltammetric detection of thrombin and adenosine, Sens. Actuat. B Chem. 160 (2011) 1380–1385.
[51] A.K.H. Cheng, B. Ge, H.-Z. Yu, Aptamer-based biosensors for label-free voltammetric detection of lysozyme, Anal. Chem. 79 (2007) 5158–5164.

[52] Y. He, D. Liu, X. He, H. Cui, One-pot synthesis of luminol functionalized silver nanoparticles with chemiluminescence activity for ultrasensitive DNA sensing, Chem. Commun. 47 (2011) 10692–10694.
[53] T. Yoshida, D. Komatsu, N. Shimokawa, H. Minoura, Mechanism of cathodic electrodeposition of zinc oxide thin films from aqueous zinc nitrate baths, Thin Solid Films 451–452 (2004) 166–169.
[54] P.S. Dorraji, F. Jalali, Novel sensitive electrochemical sensor for simultaneous determination of epinephrine and uric acid by using a nanocomposite of MWCNTs–chitosan and gold nanoparticles attached to thioglycolic acid, Sens. Actuat. B Chem. 200 (2014) 251–258.
[55] P. Klobes, K. Meyer, R.G. Munro, N.I.O. Standards, technology, porosity and specific surface area measurements for solid materials, U.S. Department of Commerce Technology Administration National Institute of Standards and Technology, 2006.
[56] M. Chen, H. Su, L. Mao, M. Guo, J. Tang, Highly sensitive electrochemical DNA sensor based on the use of three-dimensional nitrogen-doped graphene, Microchim. Acta 185 (2018) 51.
[57] L. Ribovski, V. Zucolotto, B.C. Janegitz, A label-free electrochemical DNA sensor to identify breast cancer susceptibility, Microchem. J. 133 (2017) 37–42.
[58] A. Miodek, N. Mejri, M. Gomgnimbou, C. Sola, H. Korri-Youssoufi, E-DNA sensor of mycobacterium tuberculosis based on electrochemical assembly of nanomaterials (MWCNTs/PPy/PAMAM), Anal. Chem. 87 (2015) 9257–9264.
[59] M.H. Mat Zaid, J. Abdullah, N.A. Yusof, Y. Sulaiman, H. Wasoh, M.F. Md Noh, R. Issa, PNA biosensor based on reduced graphene oxide/water soluble quantum dots for the detection of Mycobacterium tuberculosis, Sens. Actuat. B: Chem. 241 (2017) 1024–1034.
[60] P. Teengam, W. Siangproh, A. Tuantranont, T. Vilaivan, O. Chailapakul, C.S. Henry, Electrochemical impedance-based DNA sensor using pyrrolidinyl peptide nucleic acids for tuberculosis detection, Anal. Chim. Acta 1044 (2018) 102–109.